NJC

Accepted Manuscript

This is an *Accepted Manuscript*, which has been through the Royal Society of Chemistry peer review process and has been accepted for publication.

Accepted Manuscripts are published online shortly after acceptance, before technical editing, formatting and proof reading. Using this free service, authors can make their results available to the community, in citable form, before we publish the edited article. We will replace this *Accepted Manuscript* with the edited and formatted *Advance Article* as soon as it is available.

You can find more information about *Accepted Manuscripts* in the Information for Authors.

Please note that technical editing may introduce minor changes to the text and/or graphics, which may alter content. The journal's standard Terms & Conditions and the Ethical guidelines still apply. In no event shall the Royal Society of Chemistry be held responsible for any errors or omissions in this *Accepted Manuscript* or any consequences arising from the use of any information it contains.

ROYAL SOCIETY OF CHEMISTRY

www.rsc.org/njc

Journal Name New Journal of Chemistry Dynamic Article Links ►

Cite this: DOI: 10.1039/c0xx00000x

www.rsc.org/xxxxxx

ARTICLE TYPE

Agglomeration of Pd^0 nanoparticles causing different catalytic activities of Suzuki carbonylative cross-coupling reactions catalyzed by Pd^{II} and Pd^0 immobilized on dopamine-functionalized magnetite nanoparticles

Yu Long, Kun Liang, Jianrui Niu, Xin Tong, Bing Yuan, Jiantai Ma*

Received (in XXX, XXX) Xth XXXXXXXXX 20XX, Accepted Xth XXXXXXXXX 20XX
DOI: 10.1039/b000000x

Solvent-dispersible magnetite nanoparticles (Fe_3O_4) end-functionalized with amino groups were successfully prepared by a facile one-pot template-free method to immobilize Pd^{II} and Pd^0 with a metal adsorption and reduction procedure. They were characterized by TEM, XRD, XPS, FT-IR and VSM. Interestingly, Pd^{II} catalyst exhibited better catalytic activity for carbonylative cross-coupling reactions than Pd^0 catalyst. According to the catalytic activities of a variety of arylboronic acids and aryl iodides catalyzed by two kinds of Pd catalysts, proposed reaction mechanism of Suzuki carbonylative cross-coupling reactions by Pd catalyst were also inferred. More importantly, agglomeration of Pd^0 nanoparticles was obviously observed in the TEM images of the catalysts after reactions. Therefore, agglomeration of Pd^0 nanoparticles should be considered as a significant reason for different catalytic activities of the reactions catalyzed by immobilized Pd^{II} and Pd^0 catalysts. Furthermore, the Pd^{II} catalyst revealed high efficiency and stability during recycling stages.

Introduction

Synthesis of biaryl and heteroaryl carbonyl compounds has attracted considerable interest, since these compounds are important moieties in many biologically active molecules, natural products, and pharmaceuticals.[1] A variety of methods have been reported for their preparation.[2] Among them, Suzuki carbonylative coupling reaction is one of the most promising routes for the direct synthesis of biaryl ketones from carbon monoxide, as aryl halides and arylboronic acids with various functionalities can be tolerated on either partner and arylboronic acids are generally nontoxic and thermally-, air- and moisture-stable.[3] In recent years, many palladium-based homogeneous catalysts possess many merits, such as high reaction rate, high turnover number and efficient selectivity.[4] However, one of the greatest drawbacks of such catalysis is that the products might be contaminated by metalleaching.[5] Additionally, Pd is not common and cheap enough for widespread applications. So it is a big challenge to avoid Pd leach, improve the efficiency and increase recycle rate. A heterogeneous Pd-catalyst can efficiently solve these problems since heterogeneous system is facile to be handled and recovered. Therefore, supported Pd-catalysts can offer high activity and selectivity in the carbonylative coupling reactions.[6]

In recent years, there has been an increasing trend toward the use of magnetically retrievable materials in a variety of areas.[7] Fe_3O_4 as a superior magnetic material, has been used in efficient green chemical synthesis and biomedical sciences.[8] Nevertheless it was difficult to be used directly, so surface modification with active groups was indispensable for further applications. Primary amino groups may serve as functional groups suitably for the immobilization of Pd. Thus, interest in preparation of shell coated magnetic Fe_3O_4 particles functionalized with hydroxyl, carboxyl and primary amino groups is increasing dramatically.[9] Unfortunately, conventional synthetic processes of core-shell particles usually require tedious synthetic steps, long reaction time and toxic solvent. Therefore, developing a simple and facile approach to obtain functionalized magnetic materials is desperately needed.

In the past few years, dopamine (DA) had been used for surface modification of unfunctionalized Fe_3O_4 nanoparticles in the literature.[10, 5b] Among them, one-pot solvothermal synthesis dopamine-functionalized magnetite nanoparticles are promising as catalyst carrier due to their favorable solvent-dispersibility and facile template-free preparation method.[5b, 10a] DA with amino groups was used as a surfactant as well as an interparticle linker instead of using the traditional surfactants. In this paper, we stabilized Pd^{II} and Pd^0 on Fe_3O_4/DA with a metal adsorption and reduction procedure due to the covalent bonding between Pd and amine groups on the surface of Fe_3O_4/DA act as a robust anchor and avoid Pd leaching. Furthermore, the dopamine improved the dispersibility of the nanoparticles in aromatic solution. The Pd^{II} and Pd^0 catalysts were both used to catalyze Suzuki carbonylative coupling reaction under mild conditions. According to the catalytic activities of the two kinds of Pd catalysts, proposed reaction mechanism and influence factors of Suzuki carbonylative cross-coupling reactions by Pd catalyst were also inferred.

Experimental

Characterization

These magnetic materials were characterized inductively coupled plasma (ICP), powder X-ray diffraction (XRD), transmission electron microscopy (TEM), X-ray photoelectron spectroscopy (XPS), fourier transform-infrared (FT-IR) and vibrating sample magnetometry (VSM). XRD measurement was performed on a Rigaku D/max-2400 diffrctometer using Cu-Kα radiation as the X-ray source in the 2θ range of 10–80 °. The size and morphology of the magnetic nanoparticles were observed by a Tecnai G2 F30 transmission electron microscopy and samples were obtained by placing a drop of a colloidal solution onto a copper grid and evaporated in air at room temperature. Magnetic measurement of Fe_3O_4, Fe_3O_4/DA, Fe_3O_4/DA-Pd^{II} and Fe_3O_4/DA-Pd^0 was investigated with a Quantum Design vibrating sample magnetometer (VSM) at room temperature in an applied magnetic field sweeping from -15 to 15 kOe. FTIR of the MNCs was examined by using a 170SX spectrometer in the range of 400–4000 cm^{-1}. XPS was recorded on a PHI-5702 instrument and the C1s line at 284.8 eV was used as the binding energy reference.

Synthesis of the DA modified magnetic nanoparticles (Fe_3O_4/DA)

Typically[5b, 10a], $FeCl_3$ (0.973 g) was dissolved in ethylene glycol (30mL) to form a clear solution, followed by the addition of NaOAc (1.97 g) and DA (56.9 mg). The mixture was stirred vigorously for 30 min and then sealed in a Teflon-lined stainless-steel autoclave (50 mL capacity). Then the autoclave was heated to and maintained at 200 ℃ for 12 h, and allowed to cool to room temperature. The black products were washed several times with ethanol and dried at 50℃ for 24 h.

Loading of Pd^{II} on DA functionalized magnetic nanoparticles (Fe_3O_4/DA-Pd^{II})

200 mg of as-synthesised Fe_3O_4/DA nanoparticles were first dispersed in a 100mL ethanol solution under ultrasonication for 0.5 h. The formed black suspension was ultrasonically mixed with a 10 ml $PdCl_2$ (0.01 M) solution for 1 h, and then the mixed solution (0.01 M) was vigorously stirred for 2 h. The products were obtained with the help of a magnet, washed thoroughly with deionized water and ethanol then dried in a vacuum at room temperature overnight. The loading level of Pd in Fe_3O_4/DA-Pd^{II} catalyst was measured to be 3.42 % by AAS.

Loading of Pd^0 on DA functionalized magnetic nanoparticles (Fe_3O_4/DA-Pd^0)

200 mg of as-synthesised Fe_3O_4/DA nanoparticles were first dispersed in a 100mL ethanol solution under ultrasonication for 0.5 h. The formed black suspension was ultrasonically mixed with a 10 ml $PdCl_2$ (0.01 M) solution for 1 h, and then an excess 100 ml $NaBH_4$ solution (0.01 M) was slowly dropped into the above mixture with vigorous stirring. After 6 h of reduction, the products were obtained with the help of a magnet, washed thoroughly with deionized water and ethanol then dried in a vacuum at room temperature overnight. The loading level of Pd in Fe_3O_4/DA-Pd^0 catalyst was measured to be 4.17 % by AAS.

General procedure for Suzuki carbonylative coupling reactions

A mixture of aryl iodide (0.5 mmol), arylboronic acid (0.6 mmol), K_2CO_3 (1.5 mmol), and 2 mol% palladium catalyst in anisole (5 mL) was stirred at 80 ℃ under 1 atm pressure of CO. After the reaction, the mixture was cooled down to room temperature, separated by magnetic decantation, and the resultant residual mixture was diluted with 10 mL of H_2O, followed by extraction with ethyl acetate (2×10 mL). The organic fraction was dried with $MgSO_4$, the solvents were evaporated under reduced pressure and the residue was redissolved in 5 mL of ethanol. An aliquot was taken using a syringe and subjected to GC analysis. Yields were calculated against the consumption of the aryl iodides.

Result and Discussion

Catalyst preparation and characterization

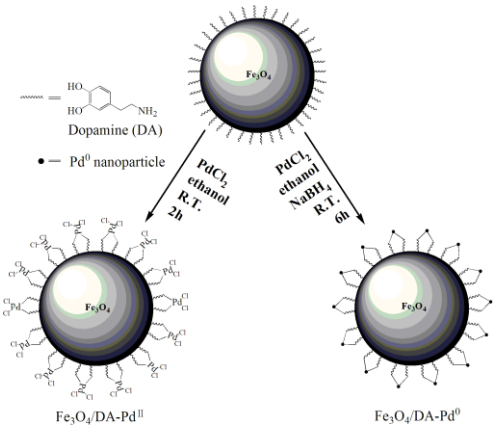

Scheme 1 Preparation of Fe_3O_4/DA-Pd^{II} and Fe_3O_4/DA-Pd^0 catalysts

The process for the preparation of Fe_3O_4/DA-Pd^{II} and Fe_3O_4/DA-Pd^0 catalysts is schematically described in Scheme 1. Briefly, Fe_3O_4/DA magnetite nanoparticles were first prepared by a facile one-pot solvothermal synthetic strategy and then immobilized Pd^{II} and Pd^0 by the amine groups on the surface of nanoparticles acting as a robust anchor and avoid Pd leaching.

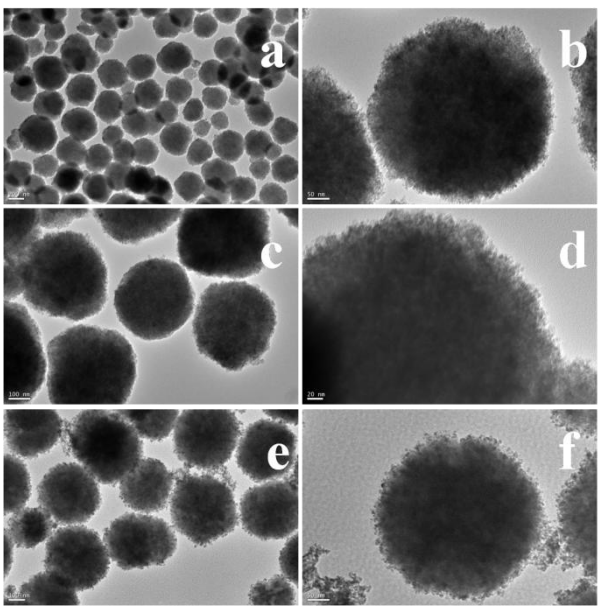

Fig. 1 TEM images of (a, b) Fe_3O_4/DA, (c, d) Fe_3O_4/DA-Pd^{II} and (e, f) Fe_3O_4/DA-Pd^0

Figures 1a and 1b show the typical TEM image of Fe_3O_4/DA nanoparticles prepared by the versatile solvothermal reaction. It could be indicated that the Fe_3O_4 modified with dopamine was highly dispersed with a spherical shape and a nearly uniform size of approximate 350 nm in diameter. The TEM image exhibited that the Fe_3O_4/DA-Pd^{II} (Fig. 1c, d,) and Fe_3O_4/DA-Pd^0 (Fig. 1e, f), catalyst didn't change considerably after attachment of the palladium onto the surface of the magnetic nanoparticles. From Figure 1c, d, it could be revealed that after fastening $PdCl_2$, no changes of the morphology of these nanoparticles had occurred, and none of Pd or PdO_x nanoparticles were observed in Fig. 1d. As shown in Figure 1e, f, it could also be concluded that the palladium particle size was cantered at about 8 nm. In order to give a powerful evidence of the existence of Pd^{II} and Pd^0, EDX spectra of Fe_3O_4/DA-Pd^{II} and Fe_3O_4/DA-Pd^0 was presented in Fig. 2. The peak of copper (Cu) arised from Cu grid in TEM analysis. The peaks corresponding to Pd were expressly found in both EDX spectra of Fe_3O_4/DA-Pd^{II} and Fe_3O_4/DA-Pd^0, and Pd content was 3.35% and 4.26%, respectively, which was almost the same with the content measured by AAS.

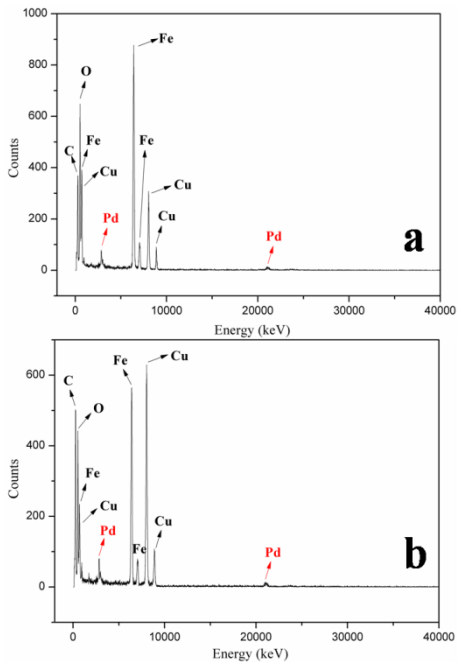

Fig. 2 EDX spectra of (a) Fe_3O_4/DA-Pd^{II} and (b) Fe_3O_4/DA-Pd^0

The crystalline structures of the resulting products were investigated by XRD. In Figure 3, the main peaks of the Fe_3O_4/DA-Pd^{II} and Fe_3O_4/DA-Pd^0 composites were similar to the Fe_3O_4/DA. The characteristic diffraction peaks in the samples at 2θ of 30.1°, 35.5°, 43.3°, 53.8°, 57.1°, and 62.8° were corresponded to the diffraction of (220), (311), (400), (422), (511) and (440) of the Fe_3O_4. All the diffraction peaks matched with the magnetic cubic structure of Fe_3O_4 (JCPDS 65-3107)[11] and the sharp and strong peaks confirmed the products were well crystallized. Figure 3c showed that apart from the original peaks, the appearance of the new peaks at 2θ= 39.8, 46.1 and 67.8 were attributed to the Pd^0 species, implying that the Pd nanoparticles had been successfully immobilized onto the surface of Fe_3O_4/DA.

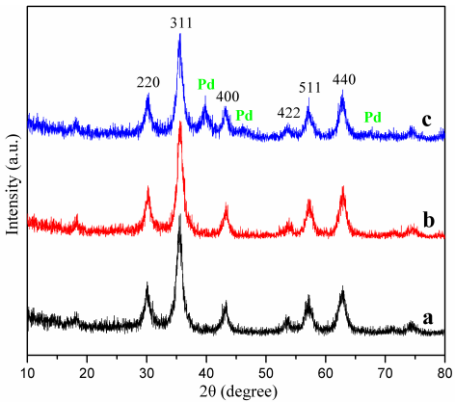

Fig. 3 XRD patterns of (a) Fe_3O_4/DA, (b) Fe_3O_4/DA-Pd^{II} and (c) Fe_3O_4/DA-Pd^0

The compositions of Fe_3O_4/DA-Pd composite were confirmed by FT-IR (Fig. 4). For comparison, FT-IR of Fe_3O_4/DA was also shown in Figure 4a. The bands at 1628, 1473 and 872 cm^{-1} were associated with amine, indicating that plenty of DA molecules were immobilized on the surface of the nanoparticles. The FT-IR spectrum of the Fe_3O_4/DA-Pd^{II} and Fe_3O_4/DA-Pd^0 catalyst (in Fig. 4b, c) demonstrated that almost no change occured after immobilization of palladium on the magnetite nanoparticle surface. Stretching vibrations took place blue shift or red shift, which exhibited $PdCl_2$ and Pd nanoparticles were fastened on the supporter.

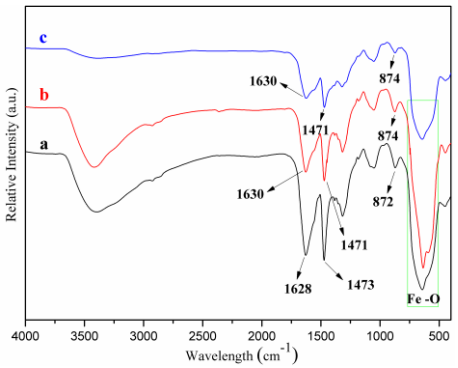

Fig. 4 FT-IR spectra of (a) Fe_3O_4/DA, (b) Fe_3O_4/DA-Pd^{II} and (c) Fe_3O_4/DA-Pd^0

Figure 5 presented XPS elemental survey scans of the surface of the Fe_3O_4/DA-Pd^{II} and Fe_3O_4/DA-Pd^0 catalyst. Peaks corresponding to oxygen, carbon, nitrogen, palladium and iron were clearly observed. To establish the oxidation state of Pd in Fe_3O_4/DA-Pd^{II} and Fe_3O_4/DA-Pd^0, XPS analysis was conducted. The Pd $3d_{5/2}$ and Pd $3d_{3/2}$ binding energies of Fe_3O_4/DA-Pd^{II} were determined to be 338.8 and 344 eV, respectively (Fig. 5b). These values agreed with the Pd^{II} binding energy of the composite. The binding energy of Pd $3d_{5/2}$ and $3d_{3/2}$ for the Fe_3O_4/DA-Pd^0 was found to be 334.8 and 340 eV (Fig. 5d), indicating that the loaded Pd nanoparticles were in its 0 state.

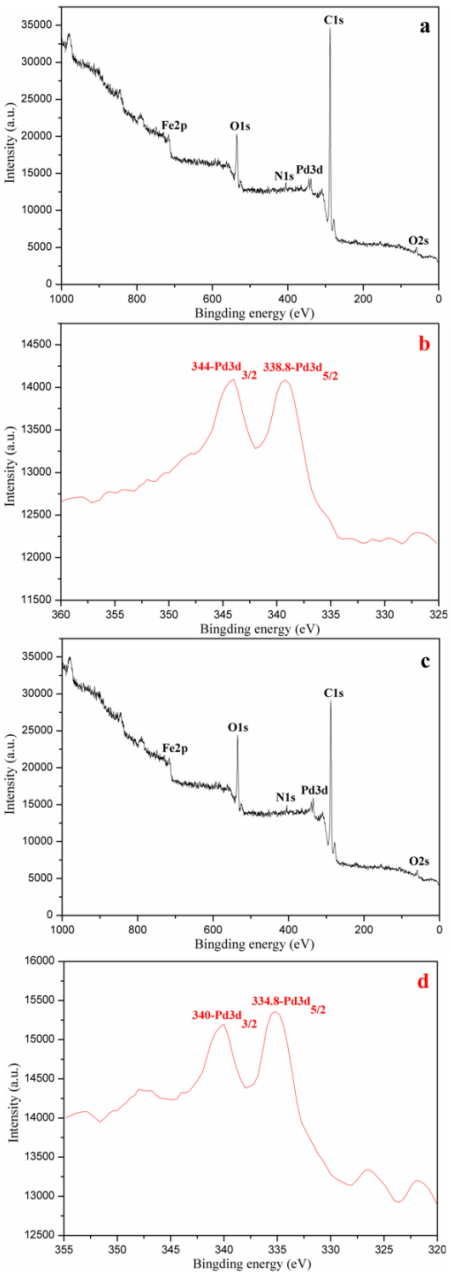

Fig. 5 XPS spectra of (a, b) Fe_3O_4/DA-Pd^{II} and (c, d) Fe_3O_4/DA-Pd^0

The magnetic properties of Fe_3O_4/DA, Fe_3O_4/DA-Pd^{II} and Fe_3O_4/DA-Pd^0 were investigated with a VSM at room temperature. As shown in Figure 6, magnetization curves revealed the superparamagnetic behaviour of the magnetic nanoparticles and the magnetic saturations of these were 81.6, 74.1 and 72.5 emu/g, respectively. The decrease of the saturation magnetization suggested the presence of Pd^{II} or Pd^0 on the surface of the magnetic support. Even with this reduction in the saturation magnetization, the nanomaterials still could be efficiently separated from the solution with a magnet near the vessels (shown in the insert in Fig. 6).

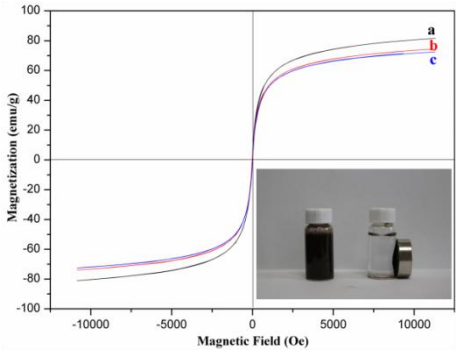

Fig. 6 Room temperature magnetization curves of (a) Fe_3O_4/DA, (b) Fe_3O_4/DA-Pd^{II} and (c) Fe_3O_4/DA-Pd^0

Catalyst testing for the Suzuki carbonylative cross-coupling reactions

In order to explore the optimal reaction conditions, including temperature, solvent and base, the carbonylative cross-coupling reaction of iodobenzene with phenylboronic acid under an atmospheric pressure of carbon monoxide was chosen as the model reaction. As shown in Table 1, the yields of the target product catalyzed by both Fe_3O_4/DA-Pd^{II} and Fe_3O_4/DA-Pd^0 were low at 40℃ and 60℃ (entry 1-4). When the temperature was increased to 80 ℃, high yields of the target product (93% and 79%) were obtained (Table 1, entry 5, 6). However, the yields of the desired product (91% and 77%) did not increase at 100℃ (Table 1, entry 7, 8). Therefore, 80 ℃ was chosen as the optimum reaction temperature. According to that both less polar solvents (anisole, dioxane and toluene) and polar solvent (DMF) obtained lower yields (Table 1, entry 9-14), non-polar solvent anisole was found to be the best choice of solvent. Under the optimized reaction temperature and solvent, several bases were examined, such as NaOAc, K_3PO_4, Cs_2CO_3 and K_2CO_3 (Table 1, entry 2, 15-20), due to the inorganic bases used in the carbonylative Suzuki coupling reaction could affect the selectivity of the products. As a result, the most used base K_2CO_3 was the most efficient base to produce carbonylative coupling product. Therefore, whether using Fe_3O_4/DA-Pd^{II} or Fe_3O_4/DA-Pd^0 as catalyst, the optimized reaction conditions are: 80 ℃, anisole, and K_2CO_3. Interestingly, it was obviously revealed that Fe_3O_4/DA-Pd^{II} always had a higher yield than Fe_3O_4/DA-Pd^0 for the carbonylative cross-coupling reaction of iodobenzene with phenylboronic acid under any reaction conditions.

In addition, the prepared Fe_3O_4/DA-Pd^{II} and Fe_3O_4/DA-Pd^0 catalysts revealed similar catalytic activities compared with literature datas on application of the amino-functionalized magnetite nanoparticles supported palladium catalysts as shown in Table 1, entry 21-24. It could be concluded that supported Pd^{II} catalysts exhibited higher catalytic activities for the carbonylative cross-coupling reaction than supported Pd^0 catalysts, so were our prepared catalysts.

Table 1 The carbonylative cross-coupling of iodobenzene with phenylboronic acid under different conditions[a].

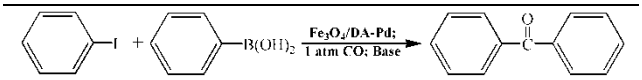

Entry	Solvent	Base	Catalyst	T/℃	Yield[b] (%)
1	Anisole	K_2CO_3	Fe_3O_4/DA-Pd^{II}	40	9
2	Anisole	K_2CO_3	Fe_3O_4/DA-Pd^0	40	3
3	Anisole	K_2CO_3	Fe_3O_4/DA-Pd^{II}	60	46
4	Anisole	K_2CO_3	Fe_3O_4/DA-Pd^0	60	35
5	Anisole	K_2CO_3	Fe_3O_4/DA-Pd^{II}	80	93
6	Anisole	K_2CO_3	Fe_3O_4/DA-Pd^0	80	79
7	Anisole	K_2CO_3	Fe_3O_4/DA-Pd^{II}	100	91
8	Anisole	K_2CO_3	Fe_3O_4/DA-Pd^0	100	77
9	Toluene	K_2CO_3	Fe_3O_4/DA-Pd^{II}	80	51
10	Toluene	K_2CO_3	Fe_3O_4/DA-Pd^0	80	42
11	Dioxane	K_2CO_3	Fe_3O_4/DA-Pd^{II}	80	76
12	Dioxane	K_2CO_3	Fe_3O_4/DA-Pd^0	80	69
13	DMF	K_2CO_3	Fe_3O_4/DA-Pd^{II}	80	55
14	DMF	K_2CO_3	Fe_3O_4/DA-Pd^0	80	52
15	Anisole	NaOAc	Fe_3O_4/DA-Pd^{II}	80	<1
16	Anisole	NaOAc	Fe_3O_4/DA-Pd^0	80	<1
17	Anisole	Cs_2CO_3	Fe_3O_4/DA-Pd^{II}	80	56
18	Anisole	Cs_2CO_3	Fe_3O_4/DA-Pd^0	80	41
19	Anisole	K_3PO_4	Fe_3O_4/DA-Pd^{II}	80	59
20	Anisole	K_3PO_4	Fe_3O_4/DA-Pd^0	80	49
21	Anisole	K_2CO_3	Fe_3O_4/PPy–Pd^{II}	80	92[c]
22	Anisole	K_2CO_3	Fe_3O_4@SiO_2-SH-Pd^{II}	80	91[d]
23	Anisole	K_2CO_3	Fe_3O_4@PNAI-Pd^{II}	80	97[e]
24	Anisole	K_2CO_3	hollow Fe_3O_4-NH_2-Pd^0	90	90[f]

a The reaction was carried out with 0.5 mmol of iodobenzene (0.5 mmol), arylboronic acid (0.6 mmol), CO (1 atm), base (1.5 mmol), solvent (5 mL), 2 mol% palladium catalyst and reaction time: 8h.

b Determined by GC or GC-MS.

c [Ref. 9e] The reaction was carried out with 0.5 mmol of iodobenzene (0.5 mmol), arylboronic acid (0.6 mmol), CO (1 atm), base (1.5 mmol), solvent (5 mL), 2 mol% palladium catalyst and reaction time: 8h.

d [Ref. 3e] The reaction was carried out with 0.5 mmol of iodobenzene (0.5 mmol), arylboronic acid (0.6 mmol), CO (1 atm), base (1.5 mmol), Pd catalyst (1 mol %) in anisole (5 mL) and reaction time: 8h.

e [Ref. 1d] The reaction was carried out with 0.5 mmol of iodobenzene (0.5 mmol), arylboronic acid (0.6 mmol), CO (1 atm), base (1.5 mmol), Pd catalyst (1 mol %) in anisole (5 mL) and reaction time: 8h.

f [Ref. 12] The reaction was carried out with 0.5 mmol of iodobenzene (0.5 mmol), arylboronic acid (0.6 mmol), CO (1 atm), base (1.5 mmol), Pd catalyst (1 mol %) in anisole (5 mL) and reaction time: 12h.

In order to investigate catalytic acivities of Fe_3O_4/DA-Pd^{II} and Fe_3O_4/DA-Pd^0 for carbonylative cross-coupling reaction, a variety of arylboronic acids and aryl iodides was tested under optimized reaction conditions, and the results were shown in Table 2. As expected, Fe_3O_4/DA-Pd^{II} always had a higher conversion and target yield than Fe_3O_4/DA-Pd^0 for the carbonylative cross-coupling reaction of iodobenzene with phenylboronic acid whether using arylboronic acids and aryl iodides containing either electron-withdrawing groups or electron-donating groups (Table 2, entry 1–30). And the carbonylative cross-coupling reactions could proceed smoothly under mild conditions to afford the corresponding carbonylative coupling products in high yields by Pd^{II} catalyst. Furthermore, it was important to receive that aryl iodides substituted with electron-withdrawing groups, such as 4-CH_3CO and 2-NO_2 (Table 2, entry 7–18), were found to be the most active reagents, since highest TOF was obtained. And since nitryl has stronger electron-withdrawing ability than acetyl, aryl iodides substituted with 4-CH_3CO had a higher TOF than aryl iodides substituted (Table 2, entry 7–18), were found to be the most active reagents, since highest TOF was obtained. And since nitryl has stronger electron-withdrawing ability than acetyl, aryl iodides substituted with 4-CH_3CO had a higher TOF than aryl iodides substituted with 2-NO_2 (Table 2, entry 7–18). In the contrast, aryl iodides substituted with electron-donating groups, such as 4-CH_3 and 4-CH_3O (Table 2, entry 19–30), exhibited relatively inferior properties. On the other hand, arylboronic acids with different substituents also afforded different yields of target products, especially, had distinct effect for the generation of by-products (Table 2, entry 1–30). It could be concluded that aryl boronic acid containing the electron-attracting group, -Cl, produced the highest yeilds of target products as well as the unacceptable direct coupling products (by-product). Meanwhile, arylboronic acid containing the electron-donating group, $–CH_3$, also showed the lowest yields of target products as well as the unacceptable by-product.

Table 2 The carbonylative cross-coupling reactions of various aryl iodides with arylboronic acids in the presence of the catalysts[a].

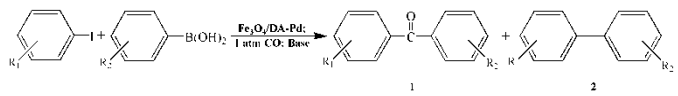

Entry	R_1	R_2	Catalyst	Time (h)	Yield[b] (%)		Conversion (%)	TOF[c] (h^{-1})
					1	2		
1	H	H	Pd^{II} [d]	8	93	5	98	5.81
2	H	H	Pd^{0} [e]	8	79	8	87	4.94
3	H	4-CH_3	Pd^{II}	8	89	3	92	5.56
4	H	4-CH_3	Pd^{0}	8	75	7	82	4.69
5	H	4-Cl	Pd^{II}	8	93	6	99	5.81
6	H	4-Cl	Pd^{0}	8	77	11	88	4.81
7	4-CH_3CO	H	Pd^{II}	6	94	3	97	7.83
8	4-CH_3CO	H	Pd^{0}	6	80	8	88	6.67
9	4-CH_3CO	4-CH_3	Pd^{II}	6	90	3	93	7.50
10	4-CH_3CO	4-CH_3	Pd^{0}	6	78	6	84	6.50
11	4-CH_3CO	4-Cl	Pd^{II}	6	91	4	95	7.58
12	4-CH_3CO	4-Cl	Pd^{0}	6	79	10	89	6.58
13	2-NO_2	H	Pd^{II}	6	96	<1	97	8.0
14	2-NO_2	H	Pd^{0}	6	83	7	90	6.92
15	2-NO_2	4-CH_3	Pd^{II}	6	92	<1	93	7.67
16	2-NO_2	4-CH_3	Pd^{0}	6	78	5	83	6.50
17	2-NO_2	4-Cl	Pd^{II}	6	95	2	97	7.92
18	2-NO_2	4-Cl	Pd^{0}	6	85	6	91	7.08
19	4-CH_3	H	Pd^{II}	8	89	3	92	5.56
20	4-CH_3	H	Pd^{0}	8	74	6	80	4.63
21	4-CH_3	4-CH_3	Pd^{II}	8	84	2	86	5.25
22	4-CH_3	4-CH_3	Pd^{0}	8	68	5	73	4.25
23	4-CH_3	4-Cl	Pd^{II}	8	88	6	94	5.50
24	4-CH_3	4-Cl	Pd^{0}	8	72	10	82	4.50
25	4-CH_3O	H	Pd^{II}	8	86	3	89	5.38
26	4-CH_3O	H	Pd^{0}	8	71	5	76	4.44
27	4-CH_3O	4-CH_3	Pd^{II}	8	79	2	81	4.94
28	4-CH_3O	4-CH_3	Pd^{0}	8	62	6	68	3.88
29	4-CH_3O	4-Cl	Pd^{II}	8	87	5	92	5.44
30	4-CH_3O	4-Cl	Pd^{0}	8	65	13	78	4.40

a The reactions were carried out with iodobenzene (0.5 mmol), arylboronic acid (0.6 mmol), CO (1 atm), K_2CO_3 (1.5 mmol), anisole (5 mL) and 2 mol% palladium catalyst.

b Determined by GC or GC-MS.

c TOF: tmoles of 1-compound yield per mole of Pd per hour.

d Fe_3O_4/DA-Pd^{II}. e Fe_3O_4/DA-Pd^{0}.

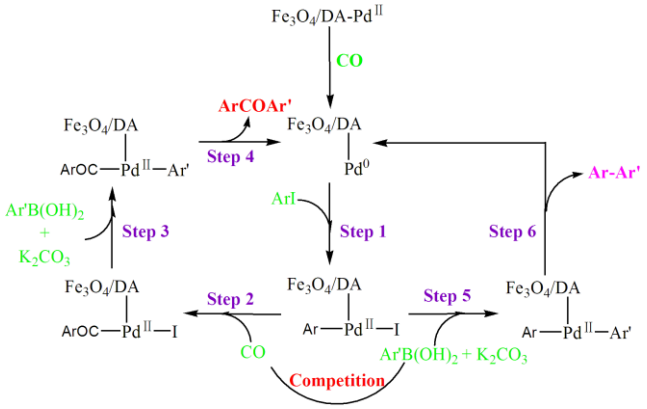

Scheme 2 The proposed reaction mechanisms for catalytic cycles of carbonylative cross-coupling reaction

In order to account for this result, according to the reaction mechanisms proposed in the literature[1d,6c,6e,9e] and combining with the results in Table 2, the proposed reaction mechanism was inferred in Scheme 2. This mechanism scheme was similar with previous, however we came up with a more particular and distinguishing exposition as followed. Firstly, in the step 1, Pd^0 was inserted to form Pd^{II} between -ph and -I. Perhaps, the existence of electron-withdrawing groups could reduce electron cloud density of the bond between ph- and I-, resulting in easier formation of bonding pair between phenyl and palladium, thus promoted the oxidative addition of Pd (0). On the contrary, the existence of electron-donating groups went against this step. Hence, aryl iodides substituted with electron-withdrawing groups exhibited higher yields than aryl iodides substituted with electron-donating groups (Table 2, entry 1–30). Secondly, intermediate product was faced with two competition processes, that was step 2 and step 5 as shown in Scheme 2. This competition process was mainly determined by the ability (or rate) of inserting CO and direct coupling with arylboronic acids. Under the same local concentration of CO, arylboronic acids substituted with electron-withdrawing groups were more likely to form direct coupling products, due to the relatively easier connection with phenyl of arylboronic acids caused by electron-withdrawing inductive effect. So, arylboronic acids substituted with electron-withdrawing groups exhibited higher yields of direct coupling products than aryl iodides substituted with electron-donating groups, while the aryl iodides substituted with electron-withdrawing groups was diametrical (Table 2, entry 1–30). Thirdly, in step 3, -I was replaced by the phenyl of arylboronic acids to form carbonylative coupling intermediate product with the aid of K_2CO_3. The substituent effect of this step was found to be similar with the step 5. Finally, in step 4 and 6, Pd^0 catalyst separated from the complex to form target product and by-product, respectively.

As shown in Scheme 2, catalytic cycles of Suzuki carbonylative cross-coupling reactions were started from the formation of Pd^0. Unfortunately, it could be apparently found that Fe_3O_4/DA-Pd^0 with Pd^0 exhibited much more inferior catalytic performance than Fe_3O_4/DA-Pd^{II} with Pd^{II} (Table 2, entry 1–30). To our best knowledge, this peculiar catalytic property could be ascribed to that Pd^0 nanoparticles are prone to conglomerate in reactions. In order to prove our conjecture, TEM images of Fe_3O_4/DA-Pd^{II} and Fe_3O_4/DA-Pd^0 after Suzuki carbonylative cross-coupling reaction

were shown in Figure 7 (a, b). Compared with Pd^0 nanoparticles of Fe_3O_4/DA-Pd^0 before the reaction (Fig. 2e, 2f), Pd^0 nanoparticles of Fe_3O_4/DA-Pd^0 after the first cycle of Suzuki carbonylative cross-coupling reaction occurred obvious agglomeration (Fig. 7b). And after 5 cycles of the reaction, the agglomeration of Pd^0 nanoparticles became more severe (Fig. 7d). To the contrary, morphology of Fe_3O_4/DA-Pd^{II} could be basically considered to maintain invariable after the reactions. It is well known that agglomeration of nanoparticles will significantly reduce the utilization of palladium, thus the relatively inferior catalytic performance of Fe_3O_4/DA-Pd^0 is acceptant.

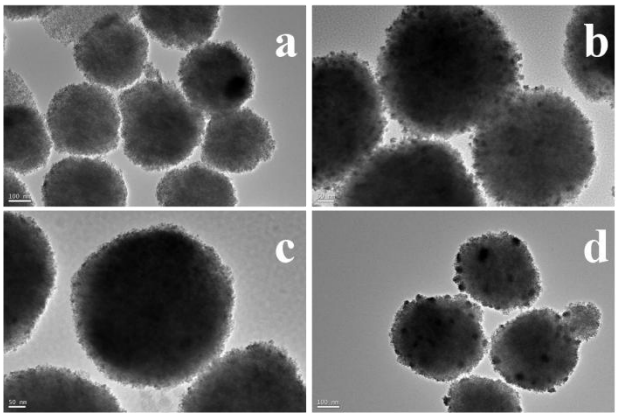

Fig. 7 TEM images of (a) Fe_3O_4/DA-Pd^{II} and (b) Fe_3O_4/DA-Pd^0 after the first cycle of Suzuki carbonylative cross-coupling reaction, (c) Fe_3O_4/DA-Pd^{II} and (d) Fe_3O_4/DA-Pd^0 after 5 cycles of the reaction

As shown in Fig. 7c, some kind of nanoparticles could be observed faintly in the TEM image of Fe_3O_4/DA-Pd^{II} after 5 cycles of the reaction, which might be Pd(0) nanoparticles as Pd(Ⅱ) should be reduced to Pd(0) to start the carbonylative cross-coupling reaction. In order to ascertain the state of the palladium in Fe_3O_4/DA-Pd^{II} after 5 cycles of the reaction, the recycled catalyst's XPS spectra had been conducted as shown in Fig. 8. It was interesting to observe three peaks assigned to Pd3d with binding energies of 334.8, 339.2 and 344 eV, respectively (Fig. 8b). The XPS result proved the existence of both Pd(Ⅱ) and Pd(0) in the Fe_3O_4/DA-Pd^{II} after 5 cycles of the reaction. This could testify the reliability of the proposed reaction mechanism in Scheme 2. On the other hand, since only a part of Pd(Ⅱ) was reduced to Pd(0), the amount of Pd^0 nanoparticles in Fe_3O_4/DA-Pd^{II} catalyst was much less than Pd^0 nanoparticles in Fe_3O_4/DA-Pd^0, which might be unable to reunite. Therefore, the agglomeration of Pd(0) nanoparticles in Fe_3O_4/DA-Pd^{II} catalyst after 5 cycles of the reaction is not obvious.

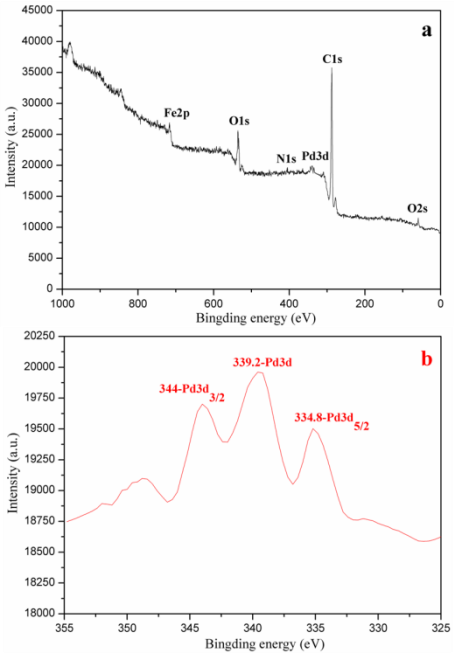

Fig. 8 XPS spectra of Fe_3O_4/DA-Pd^{II} after 5 cycles of the reaction

On the other hand, in the catalytic cycles of Suzuki carbonylative cross-coupling reactions catalyzed by Pd^{II} catalyst, Pd^{II} had to be firstly reduced to Pd^0 by CO to activate this cycle. In our opinion, this step may be a relatively fast process comparing with steps 1-6, rather than a rate determining step for the catalytic cycle. Importantly, compared with Pd^0, the extra process of reducing Pd^{II} certainly led large amount of CO to be absorbed onto the surface of catalyst, resulting in the increase of local concentration of CO. And, high local concentration of CO might be beneficial to obtain target product. Therefore, as shown in Table 2, the TOF and yields of target products catalyzed by Fe_3O_4/DA-Pd^{II} were invariably higher than that by Fe_3O_4/DA-Pd^0 no matter what substrates were tested.

Furthermore, we investigated the recyclability of the Fe_3O_4/DA-Pd^{II} and Fe_3O_4/DA-Pd^0. After the first cycle of the reaction, the catalyst was recovered with the help of a magnet, successively washed with distilled water (to remove excess of base), ethanol, and dried at room temperature ready for the next cycle. The carbonylative cross-coupling reaction of iodobenzene with phenylboronic acid catalyzed by recycled catalyst was displayed in Figure 9. After five times cycles, Fe_3O_4/DA-Pd^{II} still maintained high activity with an acceptable decrease. The weight percentage of Pd in Fe_3O_4/DA-Pd^{II} and Fe_3O_4/DA-Pd^0, determined by AAS analysis, was 3.15 % and 3.72 %, affording Pd losses of 7.8% and 10.8%, respectively. Meanwhile, after 5 cycles of the reaction, the agglomeration of Pd^0 nanoparticles was very severe (Fig. 7d). It could be concluded that the Pd^{II} of Fe_3O_4/DA-Pd^{II} was more stable than the Pd^0 of Fe_3O_4/DA-Pd^0.

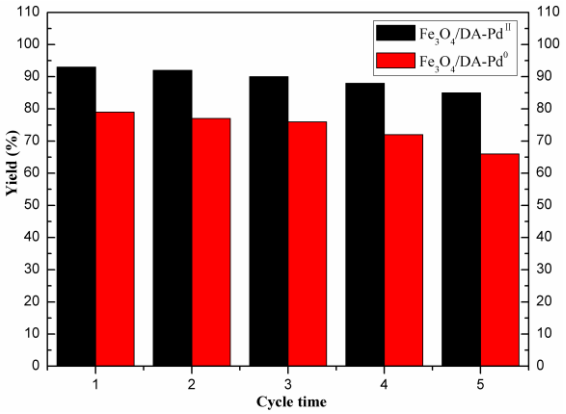

Fig. 9 Recyclability of Fe_3O_4/DA-Pd^{II} and Fe_3O_4/DA-Pd^0 for the Suzuki carbonylative cross-coupling reaction of iodobenzene with phenylboronic acid

Conclusion

In summary, Pd^{II} and Pd^0 were successfully immobilized onto Fe_3O_4/DA, which was prepared by a facile one-pot template-free method. The dopamine acted as a robust anchor, avoiding Pd leaching and improving the dispersibility of the nanoparticles in aromatic solution. Contrary to expectation, Pd^{II} catalyst exhibited better catalytic activity for carbonylative cross-coupling reactions than Pd^0 catalyst. And substituent group played an important role in the reaction. For instance, both aryl iodides and arylboronic acids substituted with electron-withdrawing groups were beneficial to improve yield of target product, unfortunately, also increase yield of direct coupling product. According to the catalytic activities of a variety of arylboronic acids and aryl iodides catalyzed by the two kinds of Pd catalysts, we came up with a particular and distinguishing exposition about the proposed reaction mechanism of Suzuki carbonylative cross-coupling reactions catalyzed by Pd catalyst. Importantly, agglomeration of Pd^0 nanoparticles was obviously observed in the TEM images of the catalysts after the reaction. And after 5 cycles of the reaction, the agglomeration of Pd^0 nanoparticles was very severe. Therefore, agglomeration of Pd^0 nanoparticles should be considered as a significant reason for different catalytic activities of the reactions catalyzed by immobilized Pd^{II} and Pd^0 catalysts. On the other hand, compared with Pd^0, the extra process of reducing Pd^{II} to Pd^0 certainly led large amount of CO to be absorbed onto the surface of catalyst, resulting in the increase of local concentration of CO. Thus, high local concentration of CO might be beneficial to obtain target product. Furthermore, the Pd^{II} catalyst revealed high efficiency and high stability during recycling stages. We envisaged that our work demonstrated an acceptable reason for the difference of catalytic activities catalyzed by supported Pd^{II} and Pd^0. It could enable further implications in a number of other heterogeneous catalytic systems as well.

Acknowledgements

The authors are grateful to The Fundamental Research Funds for the Central Universities (NO. lzujbky-2014-187), the Key Laboratory of Nonferrous Metals Chemistry and Resources Utilization, Gansu Province for financial support.

Notes

[a]State Key Laboratory of Applied Organic Chemistry, College of Chemistry and Chemical Engineering, Lanzhou University, Lanzhou, Gansu 730000, P. R. China. Fax: +86-931-891258; Tel: +86-931-8912577; E-mail: majiantai@lzu.edu.cn

References

1 (a) N. De Kimpe, M. Keppens and G. Froncg, *Chem. Commun.*, 1996, 635; (b) H. L. Li, M. Yang, Y. X. Qi and J. J. Xue, *Eur. J. Org. Chem.*, 2011, 2662; (c) P. J. Tambade, Y. P. Patil, A. G. Panda and B. M. Bhanage, *Eur. J. Org. Chem.*, 2009, 3022; (d) X. Zhu, J. Niu, F. Zhang, J. Zhou, X. Li and J. Ma, *New J. Chem.*, 2014, **38**, 4622.

2 (a) R. K. Dieter, *Tetrahedron*, 1999, **55**, 4177; (b) X. J. Wang, L. Zhang, X. Sun, Y. Xu, D. Krishnamurthy and C. H. Senanayake, *Org. Lett.*, 2005, **7**, 5593; (c) B. Hatano, J. I. Kadokawa and H. Tagaya, *Tetrahedron Lett.*, 2002, **43**, 5859.

3 (a) T. Ishiyama, H. Kizaki, T. Hayashi, A. Suzuki and N.Miyaura, *J. Org. Chem.*, 1998, **63**, 4726; (b) M. V. Khedkar, P. J. Tambade, Z. S. Qureshi and B. M. Bhanage, *Eur. J. Org. Chem.*, 2010, 6981. (c) S. Couve-Bonnaire, J. F. Carpentier, A. Mortreux and Y. Castanet, *Tetrahedron Lett.*, 2001, **42**, 3689; (d) S. Couve-Bonnaire, J. F. Carpentier, A. Mortreux and Y. Castanet, *Tetrahedron*, 2003, **59**, 2793; (e) J.-R. Niu, X. Huo, F.-W. Zhang, H.-B. Wang, P. Zhao, W.-Q. Hu, J. Ma and R. Li, *ChemCatChem*, 2013, **5**, 349.

4 (a) H. L. Li, M. Yang, Y. X. Qi and J. J. Xue, *Eur. J. Org. Chem.*, 2011, 2662; (b) M. Medio-Simon, C. Mollar, N. Rodriguez and G. Asensio, *Org. Lett.*, 2005, **7**, 4669; (c) P. Prediger, A. V. Moro, C. W. Noqueira, L. Savegnaqo, P. H. Menezes, J. B. T. Rocha and G. Zeni, *J. Org. Chem.*, 2006, **71**, 3786; (d) B. M. Okeefe, N. Simmons and S. F. Martin, *Org. Lett.*, 2008, **10**, 5301; (e) M. J. Jacinto, O. H. C. F. Santos, R. F. Jardim, R. Landers and L. M. Rossi, *Appl. Catal. A: Gen.*, 2009, **2**, 117; (f) A. J. Amali and R. K. Rana, *Green Chem.*, 2009, **11**, 1781.

5 (a) M. Cao, Y. Wei, S. Y. Gao and R. Cao, *Catal. Sci. Technol.*, 2012, **2**, 156-163; (b) J. Niu, F. Wang, X. Zhu, J. Zhao and J. Ma, *RSC Adv.*, 2014, **4**, 37761.

6 (a) S. Paul and J. H. Clark, *Green Chem.*, 2003, **5**, 635; (b) H. Q. Yang, X. J. Han, G. Li and Y. W. Wang, *Green Chem.*, 2009, **11**, 1184; (c) M. Z. Cai, G. M. Zheng, L. F. Zha and J. Peng, *Eur. J. Org. Chem.*, 2009, 1585; (d) M. Z. Cai, J. Peng, W. Y. Hao, G. D. Ding, *Green Chem.*, 2011, **13**, 190; (e) M. Z. Cai, G. M. Zheng and G. D. Ding, *Green Chem.*, 2009, **11**, 1687; (f) M. V. Khedkar, P. J. Tambade, Z. S. Qureshi and B. M. Bhanage, *Eur. J. Org. Chem.*, 2010, 6981.

7 (a) J. M. Clemente-Juan, E. Coronado and A. Gaita-Ariño, *Chem. Soc. Rev.*, 2012, **41**, 7464; (b) M. Clemente-León, E. Coronado, C. Martí-Gastaldoz and F. M. Romero, *Chem. Soc. Rev.*, 2011, **40**, 473; (c) E. Coronado and G. M. Espallargas, *Chem. Soc. Rev.*, 2013, **42**, 1525; (d) J. P. Malrieu, R. Caballol, C. J. Calzado, C. Graaf and N. Guihéry, *Chem. Rev.*, 2014, **114**, 429; (e) J. Thévenot, H. Oliveira, O. Sandre and S. Lecommandoux, *Chem. Soc. Rev.*, 2013, **42**, 7099; (f) X-Y. Wang, C. Avendaño and K. R. Dunbar, *Chem. Soc. Rev.*, 2011, **40**, 3213; (g) J. Yuan, Y. Xu and A. H. E. Müller, *Chem. Soc. Rev.*, 2011, **40**, 640.

8 (a) M. A. M. Gijs, F. Lacharme and U. Lehmann, *Chem. Rev.*, 2010, **110**, 1518; (b) J. H. Jung, J. H. Lee and S. Shinkai, *Chem. Soc. Rev.*, 2011, **40**, 4464; (c) S. Laurent, D. Forge, M. Port, A. Roch, C. Robic, L. V. Elst and R. N. Muller, *Chem. Rev.*, 2008, **108**, 2064; (d) A-H. Lu, E. L. Salabas and F. Schüth, *Angew. Chem. Int. Ed.*, 2007, **46**, 1222; (e) Y. Pan, X. Du, F. Zhao and B. Xu, *Chem. Soc. Rev.*, 2012, **41**, 2912; (f) M. B. Gawande, P. S. Branco and R. S. Varma, *Chem. Soc. Rev.*, 2013, **42**, 3371; (g) L. H. Reddy, J. Arias, J. Nicolas and P. Couvreur, *Chem. Rev.*, 2012, **112**, 5818.

9 (a) R. Abu-Reziq, D. Wang, M. Post and H. Alper, *Chem. Mater.*, 2008, **20**, 2544; (b) Y. Q. Wang, B. F. Zou, T. Gao, X. P. Wu, S. Y. Lou and S. M. Zhou, *J. Mater. Chem.*, 2012, **22**, 9034; (c) L. Gai, X. Han, Y. Hou, J. Chen, H. Jiang and X. Chen, *Dalton Trans.*, 2013, **42**, 1820; (d) V. Polshettiwar, R. Luque, A. Fihri, H. Zhu, M. Bouhrara and J. M. Basset, *Chem. Rev.*, 2011, **111**, 3036; (e) J. Niu, M. Xie, X. Zhu, Y. Long, P. Wang, R. Li and J. Ma, *J. Mol. Catal. A: Chem.*,

2014, **392**, 247; (f) J. Sun, G. Yu, L. Liu, Z. Li, Q. Kan, Q. Huo and J. Guan, *Catal. Sci. Technol.*, 2014, **4**, 1246.

10 (a) H. Zhu, C. Hou, Y. Li, G. Zhao, X. Liu, K. Hou and Y. Li, *Chem. Asian J.*, 2013, **8**, 1447; (b) M. Mazur, A. Barras, V. Kuncser, A. Galatanu, V. Zaitzev, K. V. Turcheniuk, P. Woisel, J. Lyskawa, W. Laure, A. Siriwardena, R. Boukherroub and S. Szunerits, *Nanoscale*, 2013, **5**, 2692; (c) G. Marcelo, A. Muñoz-Bonilla, J. Rodríguez-Hernández and M. Fernández-García, *Polym. Chem.*, 2013, **4**, 558; (d) A. Saha, J. Leazer and R. S. Varma, *Green Chem.*, 2012, **14**, 67; (e) G. Marcelo, A. Muñoz-Bonilla and M. Fernández-García, *J. Phys. Chem. C*, 2012, **116**, 24717; (f) K. H. Bae, Y. B. Kim, Y. Lee, J. Y. Hwang, H. W. Park and T. G. Park, *Bioconjugate Chem.*, 2010, **21**, 505; (g) D. Guin, B. Baruwati and S. V Manorama, *Org. Lett.*, 2007, **9**, 1419.

11 J.-Q. Wan, W. Cai, J.-T. Feng, X.-X. Meng and E.-Z. Liu, *J. Mater. Chem.*, 2007, **17**, 1188.

12 P. Wang, H. Zhu, M. Liu, J. Niu, B. Yuan, R. Li and J. Ma, *RSC Adv.*, 2014, **4**, 28922.